PASJ: Publ. Astron. Soc. Japan 56, 207–214, 2004 February 25

Three-Dimensional Magnetohydrodynamic Numerical Simulations of Coronal Loop Oscillations Associated with Flares

Takehiro MIYAGOSHI
Kwasan Observatory, Kyoto University, Omine-chou, Kitakazan, Yamashina-ku, Kyoto 607-8471
miyagoshi@kwasan.kyoto-u.ac.jp
Takaaki YOKOYAMA
Department of Earth and Planetary Science, The University of Tokyo, 7-3-1, Hongo, Bunkyo-ku, Tokyo 113-0033
yokoyama.t@eps.s.u-tokyo.ac.jp
and
Masumi SHIMOJO
National Astronomical Observatory, Nobeyama, Minamimaki, Minamisaku, Nagano 384-1305
shimojo@nro.nao.ac.jp

(Received 2003 August 7; accepted 2003 November 1)

Abstract

We performed three-dimensional MHD numerical simulations for solar coronal magnetic loop oscillations and found: (1) The loop oscillation period is determined by its Alfvén time. (2) The amplitude of oscillation decreases exponentially in time. This is explained as energy transport by fast-mode MHD waves. The damping rate, $\omega_{\rm damp}$, is described as $\omega_{\rm damp} \propto V_a/R$, where V_a is the Alfvén speed around loops and R is the radius of the loop. Because of computer resources limitations, the plasma β value is much larger than that of the real corona. We thus applied a scaling law derived from numerical simulation results to the real corona parameter ranges and analyzed the results.

Key words: Sun: corona — Sun: flares — Sun: magnetic fields — Sun: oscillations

1. Introduction

Coronal loop oscillations have been observed for a long time (e.g. Aschwanden et al. 1999 and references therein). There are a number of previous reports on temporal oscillations in almost all wavelengths. However, only a few are imaging observations of coronal loop oscillations, mostly restricted to one-dimensional scans (e.g., Antonucci et al. 1984; Kattenberg, Kuperus 1983; Pick, Trottet 1978; Trottet et al. 1979, 1981; Chernov et al. 1998; Sastry et al. 1981). A few two-dimensional imaging observations (e.g., Harrison 1987; Aschwanden et al. 1992; Zlobec et al. 1992) has been performed but no spatial motion of the oscillating system has been detected, probably because of insufficient spatial resolution.

The majority of these oscillations have been thought to be attributed to global modes of MHD oscillations in coronal loops. A few oscillations with periods of nearly 5 minutes have been associated with a coupling mechanism to photospheric 5-minute oscillations (e.g. Aschwanden et al. 1999). Coronal loop oscillations have been thought to be associated with coronal heating theories that involve wave interactions, e.g., resonant heating by dissipative Alfvén waves (e.g. Ionson 1978; Steinolfson, Davila 1993).

The numerical studies of coronal loops oscillations due to Alfvén waves have been performed for a long time. There has been some three-dimensional MHD modeling (e.g. Ofman et al. 1994a,b; Poedts, Goedbloed 1997). Poedts and Goedbloed studied the heating mechanism of coronal loops by the resonant absorption of incident waves.

By a data analysis of *Transition Region and Coronal Explorer* (TRACE), coronal magnetic loops oscillations that are associated with flares are detected (Aschwanden et al. 1999; Nakariakov, Ofman 2001). Observations of TRACE with high spatial resolution detected spatially oscillating loops with two-dimensional imagings. In Aschwanden et al.(1999), they studied the data of TRACE around 12:55 UT on 1998 July 14. They found some coronal loop oscillations with a flare (GOES class M4.6). The oscillating loops were most conspicuous during the first 20 minutes after the flare. The characteristics of the loop oscillations are as follows: the length of the oscillating loops is 100000 to 160000 km, the transverse amplitude of the oscillations is 2800 to 6100 km, and the mean period is 250 to 310 s. The amplitude of the transverse loop oscillations is $\sim 3\%$ of the loop length. They concluded that the oscillations were triggered by the quasi-radial propagation of the disturbance associated with the flare (the propagation speed was estimated about 700 km s^{-1}). The timing of the spatial loop displacements coincides with the arrival time of the disturbance at the loop tops. Recently, detailed analyses concerning many events have been performed (Schrijver et al. 2002; Aschwanden et al. 2002). Nakariakov et al. (1999) suggested that the amplitude decay is caused by coronal electrical diffusion. They estimated the electrical resistance by TRACE data based on this idea. Studies of coronal loop oscillations are also motivated from the view point to obtain informations about the plasma parameters (timing, velocity, density, energy, and so on) of flare-induced disturbances (e.g., Alfvénic MHD waves, shock waves, Moreton waves), and of oscillation-triggering phenomena (e.g., flare energy).

To reproduce circumstances of loop oscillation and to

investigate the damping mechanism, we carried out three-dimensional numerical MHD simulations. In this paper, we report on our results. In section 2, we provide our methods, equation system, initial conditions, and boundary conditions. In section 3, we show our simulations results. In section 4, a summary and discussions are given.

2. Numerical Simulations of Coronal Loop Oscillations

2.1. Physical Picture

We investigated coronal loop oscillations by three-dimensional MHD numerical simulations. We set a potential magnetic loop as an initial condition. As a disturbance that triggers the oscillation, we set velocity fields at the loop top and observed the decaying process of the oscillation.

2.2. Equation System

We adopt the following system of ideal MHD equations:

$$\frac{\partial \rho}{\partial t} + \nabla \cdot (\rho \boldsymbol{V}) = 0, \tag{1}$$

$$\frac{\partial}{\partial t}(\rho \boldsymbol{V}) + \nabla \cdot \left[\rho \boldsymbol{V}\boldsymbol{V} + \left(p + \frac{\boldsymbol{B}^2}{8\pi}\right)\xi - \frac{\boldsymbol{B}\boldsymbol{B}}{4\pi}\right] - \rho \boldsymbol{g} = 0, \tag{2}$$

$$\frac{\partial \boldsymbol{B}}{\partial t} + c\nabla \times \boldsymbol{E} = 0, \tag{3}$$

$$\frac{\partial}{\partial t}\left(\frac{p}{\gamma - 1} + \frac{1}{2}\rho V^2 + \frac{\boldsymbol{B}^2}{8\pi}\right) + \nabla \cdot \left[\left(\frac{\gamma p}{\gamma - 1} + \frac{1}{2}\rho V^2\right)\boldsymbol{V} + \frac{c}{4\pi}\boldsymbol{E} \times \boldsymbol{B}\right] - \rho \boldsymbol{g} \cdot \boldsymbol{V} = 0, \tag{4}$$

$$p = \frac{k_b}{m}\rho T, \tag{5}$$

$$\boldsymbol{E} = -\frac{1}{c}\boldsymbol{V} \times \boldsymbol{B}. \tag{6}$$

Here, ξ is the unit tensor; ρ, p, $\boldsymbol{V}$, k_b, m, and c are the density, pressure, velocity of fluid, Boltzman constant, mean molecular mass, and light speed, respectively. $\boldsymbol{B}$ is the magnetic field. $\boldsymbol{g}$ ($= -g\boldsymbol{e}_z$, $g = \text{const}$, $\boldsymbol{e}_z$ is a unit vector in z direction) is the gravitational acceleration, and γ ($= 5/3$) is the specific heat ratio. To make the above system of equations dimensionless, we introduce three characteristic quantities: the typical length r_0 (the major radius of the loop), the typical density ρ_0 (the density at the origin, which is the base of the corona), and the typical velocity V_{s0} (the sound speed at the origin, which is the base of the corona) in the system. We normalize all of the variables by using these three quantities and their combinations, and obtain the following dimensionless variables (primed variables):

$$\boldsymbol{r}' = \frac{\boldsymbol{r}}{r_0}, \quad \rho' = \frac{\rho}{\rho_0}, \quad \boldsymbol{V}' = \frac{\boldsymbol{V}}{V_{s0}}, \tag{7}$$

$$T' = \frac{T}{T_0} \quad \left(\text{where } T_0 = \frac{m}{\gamma k_b}V_{s0}^2\right), \tag{8}$$

$$t' = \frac{t}{r_0/V_{s0}}, \quad p' = \frac{p}{(\rho_0 V_{s0}^2)}, \tag{9}$$

$$\boldsymbol{B}' = \frac{\boldsymbol{B}}{(\rho_0 V_{s0}^2)^{1/2}}, \quad g' = \frac{g}{V_{s0}^2/r_0}. \tag{10}$$

Using these dimensionless variables, we obtain a dimensionless system of equations. After here, all physical values are dimensionless, but prime ($'$) marks are omitted.

2.3. Initial Conditions

We adopted a Cartesian coordinate system (x, y, z) in our three-dimensional formulation. The initial atmosphere is hydrostatically stratified in z:

Region 1: $T = \alpha \quad (z < z_0)$ (the photosphere/choromosphere), (11)

Region 2: $T = \alpha^{z/z_0} \quad (z_0 \le z \le 0)$ (the transition zone), (12)

Region 3: $T = 1 \quad (z > 0)$ (the corona). (13)

The parameter α ($= 0.01$) is the ratio of the temperatures of the photosphere and the corona. Note that we chose this value $\alpha = 0.01$, which is somewhat larger than a realistic one in the solar corona, where $\alpha \approx 0.005$, to save computation time. However, it has been confirmed by another run (not shown in this paper) with $\alpha = 0.005$ that the essential results are not much affected by this parameter. We took $z = 0$ at the boundary of the transition zone and the corona, and took z_0 ($= -0.2$) as the lower boundary of the transition zone. To confirm the effect of the width of transition region, we performed a calculation in which the width of transition region (z_0) was half ($= 0.1$) as large as that of the original (not shown in this paper), and found that its damping rate (mentioned in section 3) is not almost different from that of the original. We assumed this distribution of the temperature [equations (11)–(13)], and solved the hydrostatic equation,

$$-\nabla p + \rho \boldsymbol{g} = 0. \tag{14}$$

We used the solution as the initial distribution of the density and the pressure. Then, the initial distribution was expressed as follows (see figure 1):

Region 1:

$$\rho = \alpha^{-1}\exp\left[\frac{\varepsilon}{\alpha}(z_0 - z)\right]\exp\left[\frac{\varepsilon z_0}{\log\alpha}\left(\frac{1}{\alpha} - 1\right)\right], \tag{15}$$

$$p = \frac{1}{\gamma}\exp\left[\frac{\varepsilon}{\alpha}(z_0 - z)\right]\exp\left[\frac{\varepsilon z_0}{\log\alpha}\left(\frac{1}{\alpha} - 1\right)\right]. \tag{16}$$

Region 2:

$$\rho = \alpha^{-z/z_0}\exp\left[\frac{\varepsilon z_0}{\log\alpha}(\alpha^{-z/z_0} - 1)\right], \tag{17}$$

$$p = \frac{1}{\gamma}\exp\left[\frac{\varepsilon z_0}{\log\alpha}(\alpha^{-z/z_0} - 1)\right]. \tag{18}$$

Region 3:

$$\rho = \exp(-\varepsilon z), \tag{19}$$

$$p = \frac{1}{\gamma}\exp(-\varepsilon z), \tag{20}$$

where region 3 represents the corona, region 2 the transition zone, and region 1 the chromosphere and the photosphere, respectively. Here, we define the dimensionless parameter as

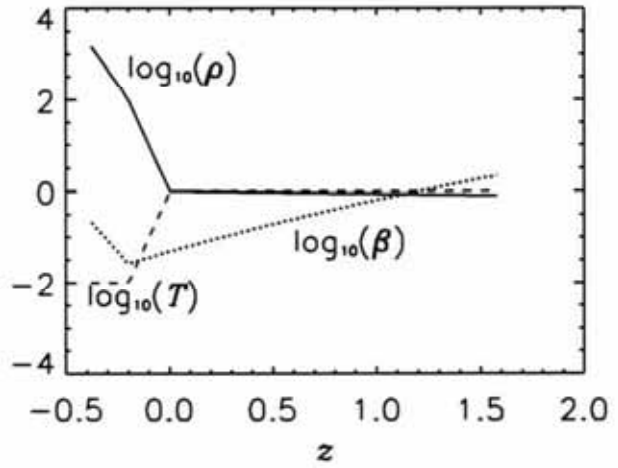

Fig. 1. Initial physical values along the $x = y = 0$ line in case 2. The vertical axis shows all physical values (solid line is $\log_{10}\rho$, dashed line is $\log_{10}T$, and dotted line is $\log_{10}\beta$). The horizontal axis shows the position.

$$\varepsilon = \frac{\gamma g r_0}{T_0} = (\gamma g'), \tag{21}$$

where ε is the ratio of the gravitational to the thermal energies.

To provide the initial potential field, we set circle current sources (e.g. Jackson 1962) with radius 1.0 at points $(x, y, z) = (\pm 1.0, 0.0, -1.5)$ (which are located out of the numerical simulation box). The strength of the circle current sources is prescribed by giving the plasma β_0 at the origin. Here,

$$\beta_0 = \frac{p_0}{B_0^2/8\pi} \tag{22}$$

is the ratio of the gas and the magnetic pressures, respectively (p_0 is the gas pressure and B_0 is the magnetic field strength at the origin). A picture of the magnetic fields distribution is given in figure 2a. The magnetic intensity as a function of z at $(x = y = 0)$ is given in figure 2c.

We set the initial velocity field with amplitude V as a perturbation to induce oscillation. The location is near the loop top (see figure 2b). We set the velocity field in the y-direction in a rectangular region ($-0.4 \le x \le 0.4$, $-0.2 \le y \le 0.2$, $0.8 \le z \le 1.2$). We performed parameter survey about V, β_0, ε, and surveyed the enhancement effect of the density of the oscillating loops, $\rho_{\rm loop}$ (see table 1). In the case 2, the value of the Alfvén speed of the oscillating loop top is $V_A = 1.35$. Thus, the Alfvén Mach number of the velocity amplitude of oscillations M_a is $\delta V/V_A \sim 0.8/1.35 = 0.6$ in case 2. Note that there is no discontinuous boundary that isolates a magnetic loop in the initial magnetic field as well as the density in cases 1 to 10. The magnetic flux that is given by the initial velocity perturbation is regarded as a 'loop' in this paper. The dense-loop case is also shown in subsection 3.2. When the unit density is $\rho_0 = 8.37 \times 10^{-16}$ [g cm^{-3}] and the unit velocity $V_{s0} = 1.66 \times 10^7$ [cm s^{-1}] in case 1, the magnetic field strength is $B \approx 8.5$ [G] at the origin (bottom of corona). At the loop top of the oscillating loops, the magnetic field strength

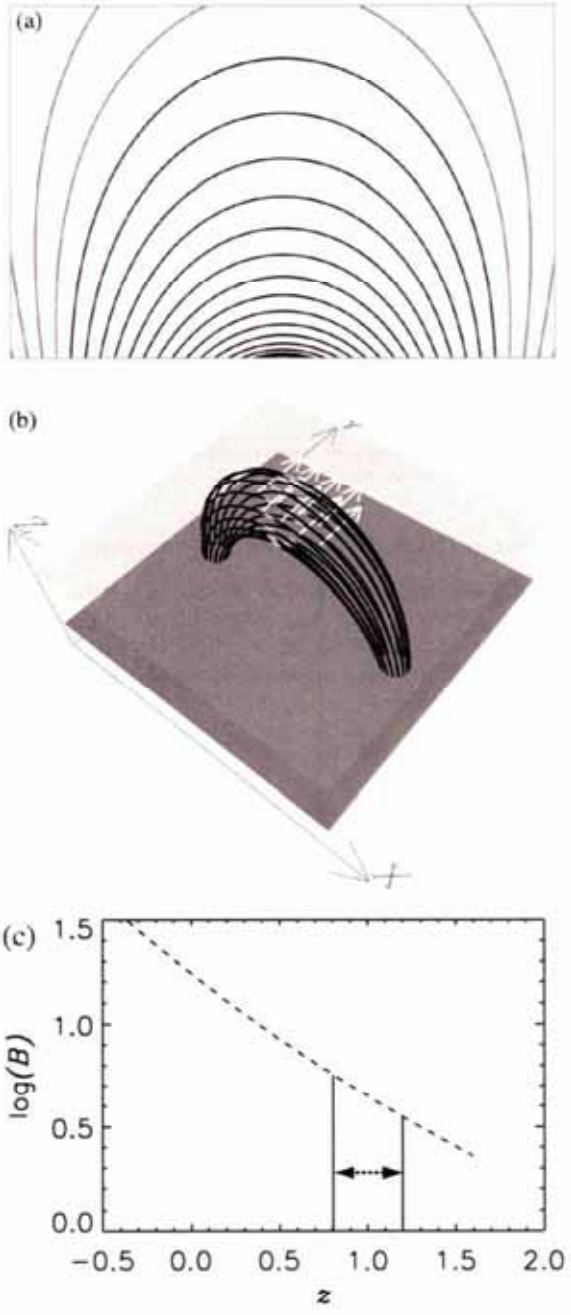

Fig. 2. (a) Magnetic fields distribution on the $y = 0$ plane. (b) A three-dimensional view of the initial magnetic lines of force (black tube) and initial inputted velocity field (white arrows) as a perturbation. A black surface shows the surface of the Sun and a gray half-opaque surface shows an iso-value surface of density ($\rho = 0.9$). (c) The magnetic intensity as a function of z at $x = y = 0$. The region indicated by the arrow shows the initial perturbed region.

is about $B = 2.6$ [G]. This is consistent with an estimation by Nakariakov and Ofman (2001) when the number density of the corona is 10^9 (figure 2 in their paper).

Table 1. Model parameters.*

Case	V	β_0	ε	$\rho_{\rm loop}$ enhancement
1	0.4	0.05	0.1	none
2	0.8	0.05	0.1	none
3	1.2	0.05	0.1	none
4	0.8	0.15	0.1	none
5	0.8	0.25	0.1	none
6	0.8	0.05	0.3	none
7	0.8	0.05	0.5	none
8	0.8	0.15	0.3	none
9	0.8	0.25	0.3	none
10	0.8	0.025	0.1	none
a	0.8	0.05	0.1	4 times
b	0.8	0.05	0.1	6 times

* Note that β_0 is defined at the origin located at the boundary between the corona and the transition region.

2.4. *Boundary Conditions and Numerical Procedures*

The simulation region is taken to be $x_{\rm min} \le x \le x_{\rm max}$ and $y_{\rm min} \le y \le y_{\rm max}$ and $z_{\rm min} \le z \le z_{\rm max}$, where $x_{\rm min} = -1.55$, $x_{\rm max} = 1.55$, $y_{\rm min} = -1.53$, $y_{\rm max} = 1.53$, $z_{\rm min} = -0.38$, and $z_{\rm max} = 1.61$. We adopt the free boundary conditions for each quantity Q at all boundaries as follows:

$$\frac{\partial Q}{\partial x} = 0 \quad (x = x_{\rm min} \text{ and } x_{\rm max}),$$

$$\frac{\partial Q}{\partial y} = 0 \quad (y = y_{\rm min} \text{ and } y_{\rm max}),$$

$$\frac{\partial Q}{\partial z} = 0 \quad (z = z_{\rm min} \text{ and } z_{\rm max}). \tag{23}$$

The number of grid points in the x, y, and z directions are 175, 159, and 132 in the simulation box, respectively. We adopted uniform mesh size from $x = -1.0$ to 1.0, $y = -0.8$ to 0.8, $z = -0.25$ to 1.5. Outside of this region, the mesh size increases by 5% of the neighboring mesh point. We solved the dimensionless system of equations by using the modified Lax–Wendroff scheme (Rubin, Burstein 1967) with an artificial viscosity (Lapidus 1967). We performed a higher-resolution calculation for the same parameters as in case 2 ($249 \times 223 \times 193$) to check the effect of the numerical viscosity. We also confirmed that the result is almost the same as that of the original.

3. Results of Numerical Simulations

3.1. *Overview*

We show an overview of our numerical results in case 2 ($\varepsilon = 0.1$, $\beta_0 = 0.05$). Figure 3 shows numerical simulation results of the time development of the three-dimensional view. It can be seen that the perturbation in the velocity fields propagates in space from the initial perturbed region not only in the direction along the loop, but also into the surrounding gas. Figures 4a1 and a2 show overviews of the oscillation on the yz plane. The magnetic loops (blue tubes) are seen from the side. The color contour shows the gas pressure and the arrows show the velocity fields. It can be seen that magnetic loops swing back and forth. The magnitude of the velocity fields decreases in time because of the fast-mode MHD wave propagation (see subsection 3.2). Figures 4b1 and b2 show an overview of the oscillation on the xy plane near the loop top ($z = 0.93$). At $t = 0.2$, the gas ahead of the oscillating loops is compressed and the induced velocity field extends widely. At $t = 2.4$, the direction of the velocity field is opposite and the amplitude becomes smaller compared with that at $t = 0.2$.

3.2. *Oscillation Periods and Damping*

Figure 5 shows the displacement of the oscillating loop (left panel) and the oscillation amplitude $(\delta V)^2$ (right panel) as functions of time t. Here, δV is the magnitude of the velocity fields at the loop top. From this numerical simulation result, it is found that, along with an oscillation, the amplitude decreases exponentially in time. It is approximately described as

$$(\delta V)^2 = (\delta V_0)^2 \exp(-\omega_{\rm damp} t) \cos\left(\frac{t}{P}\right). \tag{24}$$

Here, $\omega_{\rm damp}$ is the damping rate, P the period of the oscillation, and δV_0 the initial magnitude of the velocity fields.

Figure 6 shows the relation between the oscillation period P and the Alfvén speed of the oscillating loops at the loop top $V_{\rm A,loop}$. From this result, it is found that

$$P \propto \frac{1}{V_{\rm A,loop}}. \tag{25}$$

This result suggests that the loop oscillation is a manifestation of the Alfvén mode of the oscillating loops. Then, the period should be described as $P = 2L/V_{\rm A,loop}$, where $L = \pi$ is the loop length. The dashed line in figure 6 is a plot of this formula, which fits very well with the numerical results. The small discrepancy between the theoretical line and the data points is due to the Alfvén speed used in the model, which is measured only at a single point near to the loop apex. Actually, the Alfvén speed is non-uniform, and thus may be underestimated in the model.

Next, we discuss oscillation damping. Figure 7 shows the relation between the damping rate, $\omega_{\rm damp}$, and the plasma beta, β, at the loop top (for case 2, 4, 5, 6, 7, and 10). It is found that the damping rate, $\omega_{\rm damp}$, is described as

$$\omega_{\rm damp} \propto \frac{1}{\sqrt{\beta}}. \tag{26}$$

These results can be explained in the following discussion as energy transport by the fast-mode MHD waves propagating away from the simulation box. For simplicity, we assume that the oscillation loops are described as an oscillating board of which the thickness is w ($\sim 2R$), and the area of cross section is $S \sim (2RL)$, and the oscillation is one-dimensional. The kinetic energy (E) of the oscillation is

$$\begin{aligned} E &= \frac{1}{2}\rho_{\rm loop} \int (\delta V)^2 dv \\ &= \frac{1}{2}\rho_{\rm loop} \left[\int_{-L/2}^{L/2} (\delta V_0)^2 \cos^2 x \, dx \right] 4R^2 \\ &= \frac{1}{4}\rho_{\rm loop} (\delta V_0)^2 S w. \end{aligned} \tag{27}$$

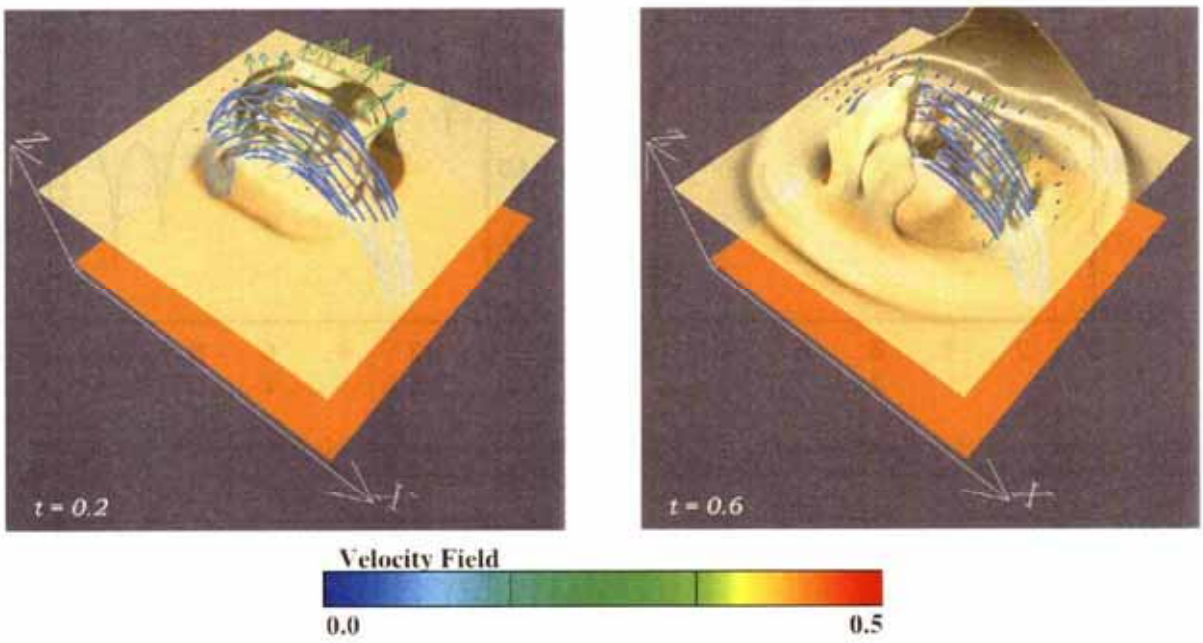

Fig. 3. Three-dimensional view of the numerical simulation results. Time evolution of magnetic lines of force (blue tube), velocity fields (arrows), and isosurface of density for $\rho = 0.9$ (a yellow half-opaque surface) in case 2. An orange surface shows the surface of the Sun.

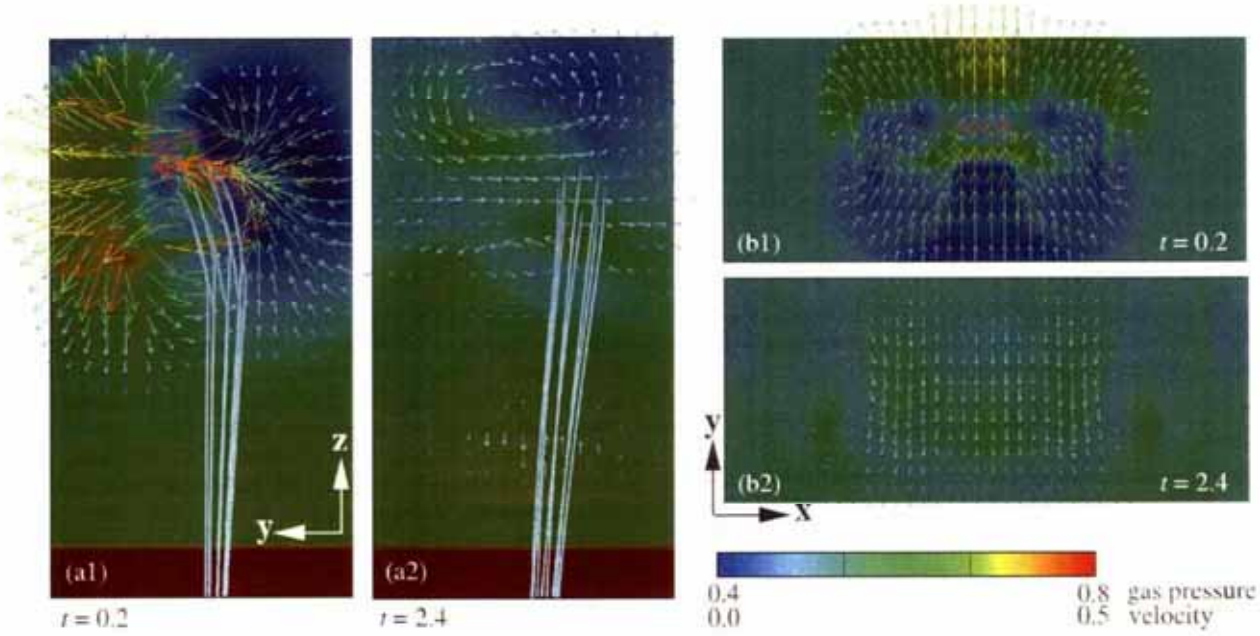

Fig. 4. Numerical simulation results: (a1)(a2) Magnetic lines of force (blue tube), velocity fields (arrows), and gas pressure (color contour on $y = 0.0$ plane) at $t = 0.2$ (a1) and at $t = 2.4$ (a2). (b1)(b2)Velocity fields (arrows) and gas pressure (color contour on $z = 0.93$ plane) at $t = 0.2$ (b1) and at $t = 2.4$ (b2).

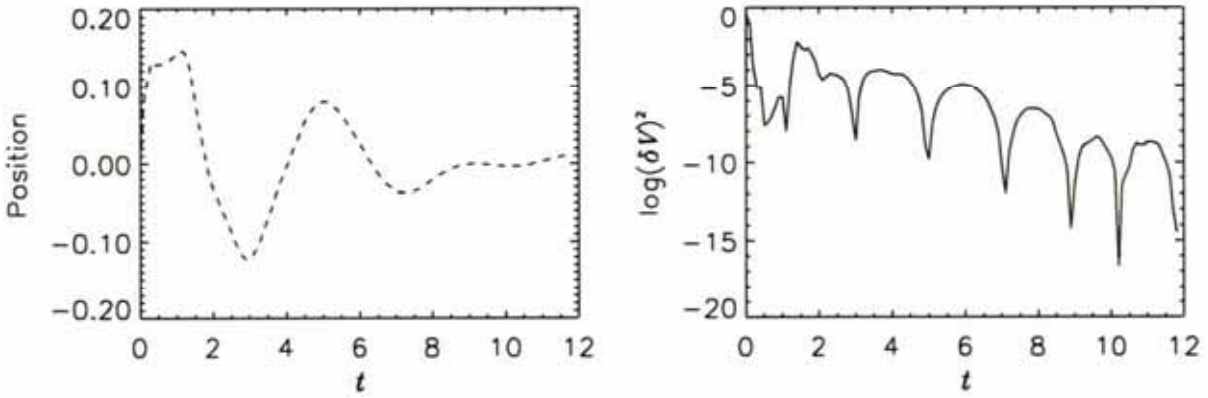

Fig. 5. (Left) Displacement of the oscillating loop (vertical axis) versus time t (horizontal axis) of case 2. (Right) The oscillation amplitude, δV^2, (vertical axis) versus time t (horizontal axis) of case 2. It is found that the amplitude decreases exponentially in time.

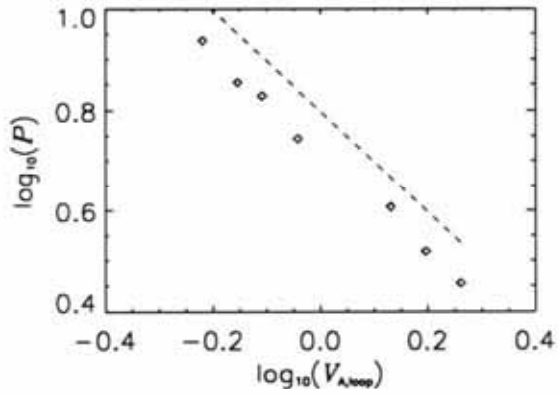

Fig. 6. Relation between P and $V_{\rm A,loop}$ (P is the oscillation period and $V_{\rm A,loop}$ is the measured Alfvén speed at the oscillating loop top for each case). It is found $P \propto V_{\rm A,loop}^{-1}$. The dashed line shows $P = 2L/V_{\rm A,loop}$.

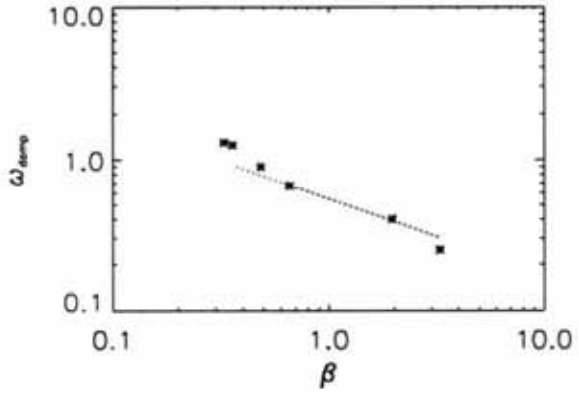

Fig. 7. Damping rate $\omega_{\rm damp}$ (vertical axis) versus plasma beta β at the loop top (horizontal axis) of case 2, 4, 5, 6, 7, and 10. It is found that the damping rate $\omega_{\rm damp}$ is described as $\omega_{\rm damp} \propto 1/\sqrt{\beta}$. The dotted line shows the theoretical line when $C_{\rm fast} = 0.3$.

Here, dv is volume element and $\rho_{\rm loop}$ is the density in the oscillating loops, respectively. The energy loss per unit time by the fast-mode MHD waves propagation is

$$\frac{dE}{dt} \sim -\rho_{\rm loop}(\delta V_{\rm fast})^2 V_{\rm f} S \sim -\rho_{\rm loop}(C_{\rm fast}\cdot\delta V)^2 V_{\rm f} S, \qquad (28)$$

where $V_{\rm f}$ is the fast-mode wave speed around the oscillating loops. We assume that the included amplitude of the fast-mode MHD wave, $\delta V_{\rm fast}$, is proportional to the oscillation amplitude, δV, by a factor, $C_{\rm fast}$, i.e. $\delta V_{\rm fast} = C_{\rm fast}\cdot\delta V$. From equations (27) and (28),

$$\frac{dE}{dt} \sim -C_{\rm fast}^2 \cdot \frac{2V_{\rm f}}{w} E \sim -C_{\rm fast}^2 \cdot \frac{2V_{\rm a}}{w} E, \qquad (29)$$

where $V_{\rm a}$ is the Alfvén mode wave speed around loops. We use the relation $V_{\rm f} \sim V_{\rm a}$ because $\beta \lesssim 1$ in the corona. From this equation, we obtain the exponentially decreasing amplitude as described in equation (24) and the damping rate ($\omega_{\rm damp}$),

$$\omega_{\rm damp} = C_{\rm fast}^2 \cdot \frac{2V_{\rm a}}{w} \sim C_{\rm fast}^2 \cdot \frac{V_{\rm a}}{R} \propto \frac{1}{\sqrt{\beta}}. \qquad (30)$$

Using the width of the perturbation region for w (= 0.4), we obtain the theoretical value for the damping rate. The dotted line in figure 7 shows this theoretical values when we take $C_{\rm fast} = 0.3$. It nearly matches the numerical simulation results.

To investigate the wave trapping effect of the dense loop (e.g. Steinolfson, Davila 1993; Ofman et al. 1994a,b), we performed calculations in which the gas of oscillating loops is denser than the surrounding one in the initial state. The density of the oscillating loops (see figure 8a) is enhanced by four (case a) or six times (case b) as large as that of case 2 in the initial state. In case b, the ratio between the Alfvén speed inside the loop ($V_{\rm A,loop}$) and outside the loop ($V_{\rm a}$) is, $(V_{\rm A,loop})/(V_{\rm a}) \sim 0.41$, which corresponds to $1/\sqrt{6}$. The Alfvén speed, $V_{\rm a}$, as a function of z at $x = y = 0$ in case b is given in figure 8b. We found that the damping rate is almost independent of the density of the oscillating loops (figure 8c) while the oscillation period increases as the density increases as $P \propto \rho_{\rm loop}^{0.3}$ (figure 8d). The dependence of the oscillation period on the density $\rho_{\rm loop}$ is understood by the decrease in the Alfvén speed of the loops. Note that the dependence is not a power

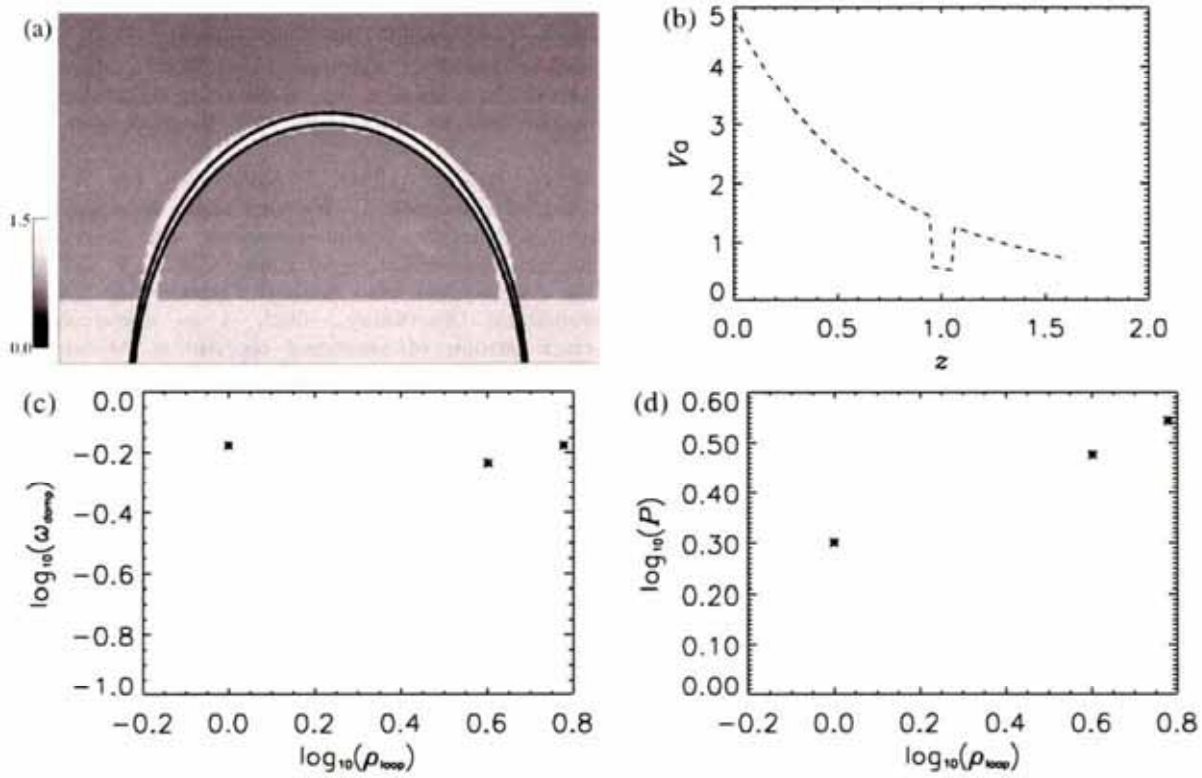

Fig. 8. (a) Density distribution of case a. The solid lines indicate the magnetic loops that are initially perturbed. (b) The Alfvén speed, V_a, as a function of z at $x = y = 0$. (c) The damping rate $\omega_{\rm damp}$ (vertical axis) versus the enhanced density $\rho_{\rm loop}$ (horizontal axis). (d) The oscillation period, P (vertical axis), versus enhanced density, $\rho_{\rm loop}$ (horizontal axis).

law with index of 0.5 because a part of the enhanced mass near the top of the oscillating loops falls down in the early period of the simulations. From these results, the theoretical model described by equation (25) is applicable, even in cases of denser loops in the shown parameter range. In other words, the trapping effect is weak in this range.

In this case only the density is enhanced in the loop, keeping other parameters all the same with case 2. So the matter is not in equilibrium and gradually falls. The temperature in the loop is lower than that of the outside by the enhanced density. The density is enhanced in the region almost tracing the oscillating loop. However, because considerable mass stayed in the loop throughout the whole calculation time, so we can see the effect of the enhanced density in the oscillation loop.

4. Summary and Discussion

We performed three-dimensional MHD numerical simulations for solar coronal magnetic loop oscillations. The results are summarized as follows: (1) The loop oscillation period is determined by its Alfvén time. (2) The amplitude of oscillation decreases exponentially in time. This is explained as energy transport by fast-mode MHD waves. The damping rate, $\omega_{\rm damp}$, is described as $\omega_{\rm damp} \propto V_a/R$, where V_a is the Alfvén speed around the loop and R is the radius of the loop. (3) The effect of the wave trapping is investigated by imposing an enhancement in the density of the oscillating loops. We found that the damping rate is almost independent of the density of the oscillating loops, while the oscillation period increases as the density increases as $P \propto \rho_{\rm loop}^{0.33}$. Therefore, the trapping effect is weak in the studied parameter range.

In this paper, we tried to explain the mechanism that controls the period and the damping of the loop oscillation. We also found that by using our results, the physical parameters of the plasma (e.g., β, Alfvén speed, and perturbation speed associated with a flare, and so on) can be estimated. For example, the result we obtained is $P = 2L/V_a$. From observations, the period is about 260 s and the loop length is about 130000 km by Aschwanden et al. (1999). We can then estimate the Alfvén speed, which is about 1000 km s^{-1} in this case. A similar estimation is also given in Nakariakov and Ofman (2001), in which they estimated the Alfvén speed.

The values of plasma β in this paper are larger than that of the real sun, because the calculation of a lower plasma β value than this is very difficult in the current computation resources. However, we obtained the relationship of equation (30) in the available parameter range. In this paper, we have presented our discussion under the assumption that this relationship is applicable even in the lower parameter range. A confirmation of this relation for realistic β values is still necessary in the future.

Nakariakov et al. (1999) mentioned that oscillation damping

may be caused by ohmic dissipation and/or by the viscosity in the corona. However, our results show that the observed damping can be explained without ohmic dissipation or viscosity. Although there is still a slight difference about the ratio of oscillation diffusion time scale to Alfvén time scale between our results and those of Nakariakov et al. (1999)'s observation, it could be explained that the oscillating loop radius, R, derived from the observation was underestimated because it was measured from the brightening visible part of the fluxes.

Coronal loop oscillations may modulate the acceleration of particles. Asai et al. (2001) observed quasi-periodic pulsations in microwaves and hard X-rays of a flare by Nobeyama Radioheliograph and Yohkoh. They found that the period of the quasi-periodic pulsations was almost equal to the global Alfvén transit time of the loop. They suggest that coronal loop oscillations may modulate the acceleration of particles. If the periods of their observation results correspond to the global Alfvén mode, it supports our estimation or Nakariakov and Ofman (2001)'s one about the periods of the oscillations.

We are grateful to Prof. T. Sakurai and Ms. A. Asai for helpful discussions. We also thank an anonymous referee for his/her helpful comments and suggestions. Numerical computations were carried out on a VPP5000 at the Astronomical Data Analysis Center of the National Astronomical Observatory, which is an inter-university research institute of astronomy operated by Ministry of Education, Culture, Sports, Science and Technology.

References

Antonucci, E., Gabriel, A. H., & Patchett, B. E. 1984, Sol. Phys., 93, 85
Asai, A., Shimojo, M., Isobe, H., Morimoto, T., Yokoyama, T., Shibasaki, K., & Nakajima, H. 2001, ApJ, 562, L103
Aschwanden, M. J., Bastian, T. S., & Gary, D. E. 1992, BAAS, 24, 802
Aschwanden, M. J., De Pontieu, B., Schrijver, C. J., & Title, A. M. 2002, Sol. Phys., 206, 99
Aschwanden, M. J., Fletcher, L., Schrijver, C. J., & Alexander, D. 1999, ApJ, 520, 880
Chernov, G. P., Markeev, A. K., Poquerusse, M., Bougeret, J. L., Klein, K-L., Mann, G., Aurass, H., & Aschwanden, M. J. 1998, A&A, 334, 314
Harrison, R. A. 1987, A&A, 182, 337
Ionson, J. A. 1978, ApJ, 226, 650
Jackson, J. D. 1962, Classical Electrodynamics (New York: Wiley), 140
Kattenberg, A., & Kuperus, M. 1983, Sol. Phys., 85, 185
Lapidus, A. 1967, J. Comp. Phys., 2, 154
Nakariakov, V. M., & Ofman, L. 2001, A&A, 372, L53
Nakariakov, V. M., Ofman, L., Deluca, E. E., Roberts, B., & Davila, J. M. 1999, Science, 285, 862
Ofman, L., Davila, J. M., & Steinolfson, R. S. 1994a, ApJ, 421, 360
Ofman, L., Davila, J. M., & Steinolfson, R. S. 1994b, Geophys. Res. Lett., 21, 2259
Pick, M., & Trottet, G. 1978, Sol. Phys., 60, 353
Poedts, S., & Goedbloed, J. P. 1997, A&A, 321, 935
Rubin, E. L., & Burstein, S. Z. 1967, J. Comp. Phys., 2, 178
Sastry, Ch. V., Krishan, V., & Subramanian, K. R. 1981, J. Astrophys. Astron., 2, 59
Schrijver, C. J., Aschwanden, M. J., & Title, A. M. 2002, Sol. Phys., 206, 69
Steinolfson, R. S., & Davila, J. M. 1993, ApJ, 415, 354
Trottet, G., Kerdraon, A., Benz, A. O., & Treumann, R. 1981, A&A, 93, 129
Trottet, G., Pick, M., & Heyvaerts, J. 1979, A&A, 79, 164
Zlobec, P., Messerotti, M., Dulk, G. A., & Kucera, T. 1992, Sol. Phys., 141, 165